X-641-69-392
PREPRINT

NUMERICAL RESEARCH FOR THE BURGERS' MODEL TURBULENCE BASED ON THE CHARACTERISTIC FUNCTIONAL FORMALISM

IWAO HOSOKAWA
KIYOSHI YAMAMOTO

SEPTEMBER 1969

GODDARD SPACE FLIGHT CENTER
GREENBELT, MARYLAND

Numerical Research for the Burgers' Model Turbulence Based on the Characteristic Functional Formalism

Iwao Hosokawa*
Goddard Space Flight Center
Greenbelt, Maryland

and

Kiyoshi Yamamoto**
National Aerospace Laboratory
Jindaiji, Chofu, Tokyo

*NASA-NRC Resident Research Associate
**National Aerospace Laboratory, Jindaiji, Chofu, Tokyo

Abstract

The one-dimensional Burgers model of turbulence is investigated by computing the functional integral expression for the correlation function, based on the Hopf theory of statistical hydromechanics, with the aid of a high-speed computer. The initial probability distribution of the velocity is assumed to be normal with zero mean and with a Gaussian covariance function. The manner in which the energy decay curve changes under variation of the Reynolds number R implies the existence of a certain asymptotic curve for $R \to \infty$. The values obtained for the correlation function at some instants indicate that the inverse-square law for the energy spectrum holds in some wave-number range for high values of R.

1. Introduction

Our last report[1] sketched briefly the method for computing the correlation function of the turbulent velocity in the Burgers fluid model,[2] using a functional integral expression. Here a full treatment of this method is presented as well as further results.

It is well known that the statistically considered Burgers equation offers insight into some of the properties of real turbulence. Our approach is to investigate the Burgers model on the basis of the Hopf theory of statistical hydromechanics,[3] with the aid of a high-speed computer where necessary. According to Hopf, the probability distribution of the velocity field u(x) at time t is given by the following characteristics functional:

$$\phi(y, t) = \int_{\Omega} \exp\left\{ i \int_{-\infty}^{\infty} y(x)\, T^t u_0(x)\, dx \right\} \delta P_0(u_0), \qquad (1.1)$$

where u_0 and y are the scalar fields in x ($-\infty < x < +\infty$); $T^t u_0(x)$ is the field which at time t has developed from the field $u_0(x)$ at time $t = 0$ according to the dynamical rule given by the Burgers equation; $P_0(u_0)$ denotes the probability distribution of u_0 at $t = 0$; and $\int_{\Omega} \delta P_0$ denotes a Lebesgue integral with the measure P_0 over the whole set Ω composed of all realizable functions $u_0(x)$. Formula (1.1) is meaningful as a solution to the turbulence problem, once P_0 is specified at the initial time and provided that the right-hand side is calculable,

since (1.1) satisfies the Hopf equation for characteristic functionals and the Hopf equation is completely equivalent to the well-known hierarchy of coupled equations for the various-order simultaneous correlation functions of the turbulent velocity field. It is easy to obtain the formula for a correlation function from (1.1). For example,

$$\left.\frac{\delta^2 \phi}{i^2\, \delta y(x_1)\, \delta y(x_2)}\right|_{y=0} = \int_\Omega T^t u_0(x_1)\, T^t u_0(x_2)\, \delta P_0(u_0)$$

$$\equiv \langle u(x_1)\, u(x_2) \rangle_t , \tag{1.2}$$

which is the two-point correlation function at time t. Here $\delta\phi/\delta y(x)$ denotes the functional derivative[3,4] of ϕ at x.

The key to making the right-hand side of (1.1) or (1.2) calculable seems to be to use a properly defined functional integration[5] to replace the abstract Lebesgue integral over a function space. Let us formally set

$$\delta P_0(u_0) = p(u_0, 0)\, \delta u_0 . \tag{1.3}$$

Here p can be understood as the probability density for the function $u_0(x)$, when $u_0(x)$ is expanded in terms of the real-valued orthonormal function set $\{s_k(x)\}$ according to

$$u_0^{2N}(x) = \sum_{k=1}^{2N} a_k\, s_k(x), \tag{1.4}$$

and δu_0 is read as

$$\delta u_0^{2N} = \prod_{k=1}^{2N} \frac{da_k}{(2\pi)^{1/2}} \quad , \tag{1.5}$$

provided, of course, that

$$\int_{-\infty}^{\infty} \cdots \int_{-\infty}^{\infty} p\,(u_0^{2N}, 0)\ \delta u_0^{2N} = 1; \qquad p \geq 0. \tag{1.6}$$

The larger the value of 2N, the more variety our function space can include. The most ideal situation would thus be reached in the limit as $2N \to \infty$. This limiting operation cannot be carried out in (1.5), because the infinite-dimensional volume element is meaningless,[6] but should be applied either to (1.3) or to the integral in (1.1). As long as this is kept in mind, we may safely use the symbolic notations which are obtained by taking the superscript 2N away from both sides of (1.4) and (1.5). Practically, however, we attempt to approximate (1.1) or (1.2) with $2N < \infty$, as described in the next section. The accuracy of approximation therefore depends on the rate of convergence to the limit, which may in turn depend on what orthonormal function set is used.

Thus, if $T^t u_0(x)$ is known explicitly in terms of u_0 and if $p(u_0, t_0)$ is properly assumed, we find no essential difficulty in proceeding with the calculation involved in (1.1) or (1.2) except that a high-speed computer is generally necessary to estimate the functional integrals needed. Indeed, for the Burgers model, Hopf[7]

and Cole's[8] general solution can be used as $T^t u_0(x)$. In the next section, the method of calculation is developed in detail on the premise that the initial probability distribution of the velocity is normal. This premise leads to the following form of initial characteristic functional:

$$\phi(y_0, 0) = \exp\left\{ i \int_{-\infty}^{\infty} U(x)\, y_0(x)\, dx - \frac{1}{2} \int_{-\infty}^{\infty} \int_{-\infty}^{\infty} Q(x, x')\, y_0(x)\, y_0(x')\, dx\, dx' \right\} , \tag{1.7}$$

where it is easy to know that the functions U and Q are the average and covariance, respectively, of the stochastic velocity field u_0 (Cf. (1.2)). We assume further

$$U(x) \equiv 0 \text{ and } Q(x, x') = e^{-(x-x')^2}, \tag{1.8}$$

i.e. the average velocity vanishes and the initial correlation function is spatially homogeneous and Gaussian. In order for the condition (1.7) to be consistent with (1.1) at $t = 0$, the function $p(u_0, 0)$ defined in (1.3) must be

$$p(u_0, 0) = \int_{\Omega} \exp\left\{ -i \int_{-\infty}^{\infty} u_0(x)\, y_0(x)\, dx \right\} \phi(y_0, 0)\, \delta y_0 . \tag{1.9}$$

(y_0 and δy_0 are understood in the same sense as described for u_0 and δu_0). The assumption of normality of the initial probability distribution is made because it can be proved from information theory[9] that this distribution is the most unbiased one, i.e. it makes the information entropy a maximum, if we have no certain

information other than U and Q. (See Appendix.) Some departure from normality may conveniently be considered by introducing a functional Gram-Charlier series, and more general assumptions for U and Q may also be used if necessary. However, the present research is confined within the limits set by the above premise, since our main purpose is to verify the practicability of our fundamental approach.

2. Method of Calculation

i) Diagonalization of the normal probability density

We first calculate (1.9) in order to obtain a simple explicit form of (1.3). This can be achieved by a transformation of the coordinate frame of the function space. To correspond with (1.4), let us start from the expression

$$y_0^{2N}(x) = \sum_{i=1}^{2N} a_i \, s_i(x). \tag{2.1}$$

At $x = x_m$ $(m = 1, \ldots, 2N)$, we set

$$y_0^{2N}(x_m) = \frac{1}{\pi^{1/2}} \sum_{j=1}^{N} \{\eta(k_j) \cos k_j x_m + \zeta(k_j) \sin k_j x_m\} \Delta k_j, \tag{2.2}$$

where Δk_j is the length of the j th interval when the number range $(0, \infty)$ is divided to N intervals, and k_j is the representative value of k in the j th interval. The 2N simultaneous equations obtained by equating the right-hand-sides of (2.1) and (2.2) for each value of m give a one-to-one correspondence between $(a_1, \ldots, a_{2N})$ and $(\eta(k_1)(\Delta k_1)^{1/2}, \ldots, \eta(k_N)(\Delta k_N)^{1/2}, \zeta(k_1)(\Delta k_1)^{1/2}, \ldots, \zeta(k_N)(\Delta k_N)^{1/2})$. If we multiply these 2N equations on both sides by $s_n(x_m)\Delta x_m$, where Δx_m is an interval about the representative point x_m of such length that the sum of all disjoint Δx_m covers the whole x space, and if we then sum over m, we obtain

$$a_n = \frac{1}{\pi^{1/2}} \sum_{j=1}^{N} \left\{ \eta(k_j) \int_{-\infty}^{\infty} s_n(x) \cos k_j x \, dx \right.$$

$$\left. + \zeta(k_j) \int_{-\infty}^{\infty} s_n(x) \sin k_j x \, dx \right\} + \epsilon \qquad (2.3)$$

by the properties of orthonormal functions. Here ϵ is a quantity which tends to zero as all $\Delta x_m \to 0$ (i.e. as $2N \to \infty$). The Jacobian of the transformation is calculated as follows:

$$\frac{\partial a_i}{\partial \{\eta(k_j)(\Delta k_j)^{1/2}\}} = \left(\frac{\Delta k_j}{\pi}\right)^{1/2} \int_{-\infty}^{\infty} s_i(x) \cos k_j x \, dx + 0(\epsilon) \equiv t_{ij}, \qquad (2.4)$$

$$\frac{\partial a_i}{\partial \{\zeta(k_j)(\Delta k_j)^{1/2}\}} = \left(\frac{\Delta k_j}{\pi}\right)^{1/2} \int_{-\infty}^{\infty} s_i(x) \sin k_j x \, dx + 0(\epsilon) \equiv t_{i,N+j}. \qquad (2.5)$$

Hence we have

$$\sum_{j=1}^{N} (t_{ij}\, t_{\ell j} + t_{i,N+j}\, t_{\ell,N+j}) = \frac{1}{\pi} \int_{-\infty}^{\infty} \int_{-\infty}^{\infty} dx\, dx' \left[s_i(x)\, s_\ell(x') \right.$$

$$\left. \cdot \sum_{j=1}^{N} (\cos k_j x \cos k_j x' + \sin k_j x \sin k_j x') \Delta k_j \right] + 0(\epsilon)$$

$$= \delta_{i\ell} + 0(\epsilon) + \epsilon' \qquad (2.6)$$

where δi_ℓ is the Kronecker symbol and the quantity ϵ' tends to zero as all $\Delta k_j \to 0$ (i.e. as $N \to \infty$). This indicates that the transformation of the representation of the function space from $(a_1, \ldots, a_{2N})$ to $(\eta(k_1)\,(\Delta k_1)^{1/2}, \ldots, \eta(k_N)\,(\Delta k_N)^{1/2}, \zeta(k_1)\,(\Delta k_1)^{1/2}, \ldots, \zeta(k_N)\,(\Delta k_N)^{1/2})$ is orthogonal in the limit $N \to \infty$. Accordingly, δy_0 may be expressed in our symbolic sense as

$$\delta y_0 = \prod_i d\eta(k_i) \left(\frac{dk_i}{2\pi}\right)^{1/2} d\zeta(k_i) \left(\frac{dk_i}{2\pi}\right)^{1/2} . \tag{2.7}$$

At the same time, (2.2) reduces for almost all x to

$$y_0(x) = \frac{1}{\pi^{1/2}} \int_0^\infty \{\eta(k) \cos kx + \zeta(k) \sin kx\}\, dk . \tag{2.8}$$

If we introduce the relations

$$\eta(k) = \frac{z(k) + z(-k)}{2^{1/2}} , \quad \zeta(k) = \frac{i\{z(k) - z(-k)\}}{2^{1/2}} , \tag{2.9}$$

(2.8) may be rewritten as

$$y_0(x) = \frac{1}{(2\pi)^{1/2}} \int_{-\infty}^{\infty} z(k)\, e^{ikx}\, dk , \tag{2.10}$$

where $z^*(k) = z(-k)$, the asterisk denoting the complex conjugate. With the aid of these relations the quadratic form in (1.7) can be rewritten in a diagonal form as

$$\frac{1}{2}\int_{-\infty}^{\infty}\int_{-\infty}^{\infty} Q(x-x')\, y_0(x)\, y_0(x')\, dx\, dx' = \frac{1}{2}\int_{-\infty}^{\infty} \sigma(k)\, z(k)\, z(-k)\, dk$$

$$= \frac{1}{2}\int_{0}^{\infty} \mathrm{Re}\,\sigma(k)\,\{\eta^2(k) + \zeta^2(k)\}\, dk \qquad (2.11)$$

where Re indicates the real part and $\sigma(k)$ is the Fourier component of Q(x), which when calculated from (1.8) is found to be

$$\sigma(k) = \int_{-\infty}^{\infty} Q(x)\, e^{ikx}\, dx = \pi^{1/2}\, e^{-k^2/4} \,. \qquad (2.12)$$

To make possible the calculation of the functional integral in (1.9), we introduce a modified Fourier expansion of $u_0(x)$ as follows:

$$u_0(x) = \frac{1}{\pi^{1/2}}\int_{0}^{\infty} [\mathrm{Re}\,\sigma(k)]^{1/2}\,\{\Lambda(k)\cos kx + M(k)\sin kx\}\, dk\,. \qquad (2.13)$$

Hence, we can compute

$$\int_{-\infty}^{\infty} y_0(x)\, u_0(x)\, dx = \int_{0}^{\infty} [\mathrm{Re}\,\sigma(k)]^{1/2}\,\{\Lambda(k)\,\eta(k) + M(k)\,\zeta(k)\}\, dk, \qquad (2.14)$$

and finally can arrive at the formula

$$p(u_0,\ 0) = \exp\left[-\frac{1}{2}\sum_{j}\{\Lambda^2(k_j) + M^2(k_j)\}\, dk_j\right] \prod_{j}\left\{\frac{1}{\mathrm{Re}\,\sigma(k_j)}\right\}. \qquad (2.15)$$

Now δu_0 may be expressed in the same way that δy_0 is expressed in (2.7). If (2.13) is compared with (2.8), it is seen that the proper expression is

$$\delta u_0 = \prod_j \left\{ [\mathrm{Re}\ \sigma(k_j)]^{1/2}\, d\Lambda(k_j) \left(\frac{dk_j}{2\pi}\right)^{1/2} [\mathrm{Re}\ \sigma(k_j)]^{1/2}\, dM(k_j) \left(\frac{dk_j}{2\pi}\right)^{1/2} \right\} . \tag{2.16}$$

These last two equations now provide a simple, explicit, direct-product form for (1.3):

$$p(u_0, t_0)\delta u_0 = \exp\left[-\frac{1}{2} \sum_j \{\Lambda^2(k_j) + M^2(k_j)\}\, dk_j\right] \cdot \prod_j \left\{ d\Lambda(k_j) \left(\frac{dk_j}{2\pi}\right)^{1/2} \cdot dM(k_j) \left(\frac{dk_j}{2\pi}\right)^{1/2} \right\} \tag{2.17}$$

which demonstrates that the stochastic variables $\{ A(k_j)\, dk_j^{1/2}\, ,\ M(k_j)\, dk_j^{1/2}\}$ distribute standard-normally, independently of each other. It is worth noting that (2.17) is just the Gaussian measure on the function set of $\Lambda(k)$ cross $M(k)$ established by Friedrichs,[10] so that (1.1) or (1.2) is just a functional integral with the Gaussian measure, the integrand of which is a functional of $\Lambda(k)$ and $M(k)$ through the relation (2.13).

ii) Monte Carlo quadrature

For the Burgers fluid model, $T^t u_0$ in (1.1) or (1.2) can be written as

$$T^t u_0 = \frac{\int_{-\infty}^{\infty} (x - x') \exp\left\{-\frac{R}{2}\int_0^{x'} u_0(x'')\,dx'' - \frac{R(x-x')^2}{4t}\right\} dx'}{t\int_{-\infty}^{\infty} \exp\left\{-\frac{R}{2}\int_0^{x'} u_0(x'')\,dx'' - \frac{R(x-x')^2}{4t}\right\} dx'} \qquad (2.18)$$

(the Hopf-Cole solution[7,8]); this satisfies the dimensionless Burgers equation,

$$\frac{\partial u}{\partial t} = -u\frac{\partial u}{\partial x} + \frac{1}{R}\frac{\partial^2 u}{\partial x^2}\ , \qquad (2.19)$$

where R is the Reynolds number referred to the initial characteristic correlation length and the root-mean-square value of the initial velocity (Cf. (1.8)).

In order to estimate the functional integral (1.2) for any values of x_1, x_2, and t, it is most convenient to use the Monte Carlo quadrature for a multiple integral[11] on an approximate basis such that Δk_j and N are kept finite in a proper way. That is, we will use the so-called cylinder functional approach. Estimation of (1.2) then reduces to the averaging of many sample values of $T^t u_0(x_1)\, T^t u_0(x_2)$ (called the estimator[11]) which corresponds to taking many sets of 2N independent standard-normal random numbers as values for the variables $\{\Lambda(k_j)\, dk_j^{1/2}\ ,\ M(k_j)\, dk_j^{1/2}\}$.

Thus, (2.13) may be replaced by

$$u_0(x) \cong \frac{1}{\pi^{1/4}} \sum_{j=1}^{N} e^{-k_j^2/8} \{\Lambda(k_j) \cos k_j x + M(k_j) \sin k_j x\} \Delta k; \tag{2.20}$$

here (2.12) was substituted for $\sigma(k)$ and all Δk_j were put equal to Δk so that $k_j = (j - 1/2)\Delta k$. The maximum wave-number k_c to be considered for $u_0(x)$ is given by $k_c = N\Delta k$. The value of k_c, which is chosen so as to make the error of (2.20) due to the neglect of higher wave components less than 1%, may be determined from the equation

$$\int_{k_c}^{\infty} e^{-k^2/8} dk \Big/ \int_0^{\infty} e^{-k^2/8} dk \doteq 1/100, \tag{2.21}$$

which yields $k_c \doteq 5.17$. Once k_c is fixed, Δk depends on N. The question of how large N should be was discussed in our last report;[1] results presented herein are given for values of N as large as 30 and even 45 to insure convergence. The larger $N = k_c/\Delta k$ is, of course, the smaller is the error due to using the rectangle rule as an approximation to the integral expression (2.13). Using (2.20), the integral over x'' in (2.18) may be expressed as

$$\int_0^{x'} u_0(x'')\, dx'' \cong \frac{1}{\pi^{1/4}} \left[\sum_{j=1}^{N} \frac{e^{-k_j^2/8}}{k_j} \{\Lambda(k_j) \sin k_j x' - M(k_j) \cos k_j x' + M(k_j)\} \Delta k \right].$$

But, in the case where Δk is not necessarily small, the alternative expression

$$\int_0^{x'} u_0(x'')\,dx'' \cong \frac{1}{\pi^{1/4}} \sum_{j=1}^{N} \frac{e^{-k_j^2/8}}{k_j} \left[\left\{ \Lambda(k_j) \sin k_j x' - M(k_j) \cos k_j x' \right\} \frac{\sin \Delta k x'/2}{x'/2} + M(k_j)\,\Delta k \right] \qquad (2.22)$$

is much more efficient. Indeed, the factor $\sin\Delta k\,(x'/2)/(x'/2)$ prevents the deterioration of the Monte Carlo quadrature caused by a large vibration of sample values for a large value of x'. The integrals of both the numerator and the denominator of (2.18) were calculated by the Simpson rule, using (2.22). In this calculation there are two points to be noted. First, the exponential function in the integrands should be normalized to a value as close to its maximum value as is possible, because at some times it becomes enormously large and at other times infinitesimally small. Second, the interval of integration cannot be infinite in practice, so that integration is stopped at the points where the integrands decrease to less than 10^{-7} times their maximum value, taking account of the rather rapid, monotonic decrease of the factor $\exp\{-R(x - x')^2/4t\}$ for $|x'|$ large. For convenience, a new variable, $s \equiv (R/4t)^{1/2}\ (x - x')$, was introduced in place of x'. The accuracy of our Simpson numerical integration may be judged by the fact that the value of the integral was unchanged except for the fourth digit when the integration step length was decreased by a factor of 2. Examples of the calculation of (2.18) are given in Figs. 8 and 9.

Our standard-normal random numbers were generated by the simple but highly reliable method of Kronmal.[12] The number of sample values for the estimator in our Monte Carlo quadrature was between 300 and 500. The reliability of this quadrature may be judged from the examples shown in Figs. 2 and 4.

3. Results and Discussion

i) Features of the energy decay

In Fig. 1, twice the calculated dimensionless energy of turbulence, $\langle [u(0)]^2 \rangle_t$, is plotted against the dimensionless time (normalized with the initial characteristic correlation length divided by the root-mean-square of the initial velocity field) for various Reynolds numbers. The Monte Carlo quadrature was done with N = 30, and the number of samples is 300. The solid lines show the corresponding results from the linear theory, $\langle [u(0)]^2 \rangle_t = 1/(1 + 8t/R)^{1/2}$, where the non-linear term in the Burgers equation is neglected. The dotted line gives the corresponding results from the approximate theory of Meecham and Siegal[13] for R = 100. The reliability (or stability) of our Monte Carlo quadrature is indicated by Fig. 2, which shows how the value of the integral depends on the number of samples taken in the case R = 100.

Considering the approximate nature of Monte Carlo quadrature, the agreement between our results and the linear theory for R = 0.1 and 1 is excellent at the initial time; but after the energy has decayed to one-tenth of its initial value, our results begin to deviate from those of the linear theory, giving rise to a little more rapid decay. This seems to be due to a nonlinear effect which transfers energy from the small wave-number components to larger wave-number components, where viscous dissipation is stronger.

For R greater than 10, the character of the energy decay is quite different from that expected on the basis of the linear theory. Even more interesting,

the plotted points suggest the existence of an asymptotic curve for $R \to \infty$. Indeed, the points plotted for R = 100 seem already to represent the features of the asymptotic curve to good accuracy. (Cf. those for R = 1000.) As can be seen, the theoretical curve of Meecham and Siegal deviates considerably from this expected asymptotic curve. Their approach is based on the Wiener-Hermite expansion of the random field u(x), but with some drastic assumptions in order to avoid an open hierarchy of unknown functions and other complexities involved with the calculation, whose validity was questioned by Orszag and Bissonnette.[14]

In Fig. 3, the manner in which the result depends on N is shown for the case of R = 100. The data for N = 15 were also presented in our last report; there, on the basis of a comparison with the data for N = 10, it was argued that the N = 15 data accurately represent the solution in terms of the functional integral (1.2). This comparison, however, was not satisfactory because the values of k_c for the two cases were considerably different. As can be seen in Fig. 3, the data for N = 15 are still rather far from the expected limiting values for $N \to \infty$ with the fixed value of k_c given by (2.21). It appears that the data for N = 30 are much nearer the limiting values. This indicates that the accuracy of the present calculation is higher than before.

There are some arguments to the effect that the energy of the (spatially periodic) Burgers' model turbulence should decay like t^{-2} in the limit $R \to \infty$, if t is large enough.[15] Our results for large N include no symptom of decay like t^{-2}, at least up to t = 100. However, we do see symptoms of such a rapid decay

for small values of N. (See Fig. 3.) The smallness of N means that the initial velocity fields are restricted to a considerably small class of the function space Ω, as is known from (2.20). For the ensemble of such a relatively simple class of initial velocity fields, the saw-tooth wave argument[15] appears to be easily realizable, because (2.20) then has the nature of a velocity field which is strongly spatially periodic (relative to the initial characteristic length of correlation). But the larger N is, the larger the class of initial velocity fields involved is, and the more difficult it is to realize the so-called saw-tooth wave argument, in a short time, at least. Here it is worth recalling that there exists a similarity solution of the Burgers equation which has the shape of a solitary wedge with the hinge point fixed on the x axis, and that the energy of this velocity field decays not like t^{-2} but rather like $t^{-1/2}$.[2] If this type of velocity field comes into the ensemble, obviously the rapid decay based on the saw-tooth wave argument should be reconsidered. There might be various other solutions with different decay patterns. In the limit as $N \to \infty$ the ensemble should include all these solutions. This fact seems to give theoretical support to the present result of a rather slow decay of the energy. It is most interesting to note that in the later period of decay ($t > 3$) our result is close to Burgers' prediction,[2] based on a statistical assumption, of a $t^{-2/3}$ dependence. Burgers assumes that during the intermediate period of the decay, the velocity field over the infinite domain may be approximated for large R by a series of discontinuous straight-line segments of positive slope which decreases with time but of random length and random magnitude

of drop from one segment to another. He also takes into account frequent coalescence of discontinuous points, i.e. shocks.

The final result obtained of course would depend on what ensemble of velocity fields is taken initially, i.e. what is prescribed as $\phi(y_0, 0)$. Our choice is indicated by (1.7)-(1.8); and, as we have already said on an information-theoretical basis, this ensemble is the one most often realizable, unless we have other peculiar information. If N is too small, it is obvious that the calculation cannot give an exact result for this initial ensemble, since in that case the functional integration has been carried out imperfectly.

ii) Correlation function and energy spectrum

The correlation function $\langle u(0)u(x)\rangle_t$ was calculated at t = 1 for R = 1000, at t = 1 and 3 for R = 100 and at t = 1 for R = 1, as is shown in Fig. 4. The solid line is the curve at t = 0, i.e. $Q(x) = e^{-x^2}$. The dotted lines are the theoretical results of Meecham and Siegel[13] at t = 1 and 3 for R = 100. The reliability of our Monte Carlo quadrature is observed in Fig. 5, where the number of samples was taken up to 500.

Fig. 4 shows the general trend of the correlation function to become flatter and flatter as time goes on. As expected from the observation in the preceding subsection, there is so little difference between the correlation functions at the same instant t = 1 for R = 100 and R = 1000 that they are considered to represent the asymptotic curve of the correlation function for $R \to \infty$. However, the

correlation function at the same t for R = 1 is very different from that for a higher Reynolds number; it becomes flat faster than the latter, because of the stronger viscous dissipation. It may be seen from the figure that the correlation function at t = 1 for R = 1 is quite similar to that at t = 3 for R = 100, which contains a comparable amount of turbulence energy. But the fact that these two curves cross each other somewhere between x = 1.0 and x = 2.0 with different curvatures seems to suggest some delicate structural difference between them. This may be clarified by comparing their energy spectrums.

The energy spectrum corresponding to each correlation function can be calculated from the equation

$$E(k, t) = \frac{1}{\pi} \int_0^\infty \cos kr \cdot Q(r, t)\, dr, \tag{3.1}$$

where $Q(r, t) = \langle u(0)\, u(r) \rangle_t$. The curve of Q(r, t) was made by connecting the plotted points in as smooth a way as possible, but the result of numerical calculation for E(k, t) (using Filon's method[16]) predicted not a smooth curve but a somewhat rugged curve, as shown in Fig. 6. This seems to be an unavoidable effect caused by the error inherent in Monte Carlo quadrature. Nevertheless, it is interesting to note that there is an appreciable region of the energy spectrum in which the slope is very nearly k^{-2} for R = 100 at both t = 1 and t = 3. It is evident from the figure that this well-discussed feature of the energy spectrum

of the Burgers' model turbulence[2,13,15,17] appears in a very short time and is kept pretty long for R = 100, while the same feature is barely observable at t = 1 for R = 1. This contrast between the energy spectrum at t = 3 for R = 100 and that at t = 1 for R = 1 explains to some degree the above-described structural difference between the correlation functions for these two cases. We may understand this fact from the nonlinear effect of the Burgers equation; indeed, without the strong nonlinear interaction the energy in high wave-number regions would decay almost according to $e^{-2k^2 t/R}$, while if the energy transfer from lower to higher wave-number regions of the spectrum occurs through the nonlinear interaction, the effect of the relatively strong energy decay of the high wave-number components will be considerably mitigated so that the k^{-2} spectrum law may be recovered in some range of k, which may be called the inertial range.

As shown in Fig. 4, Meecham and Siegel's theoretical results are different from our results at t = 1 and 3 for R = 100; but from the viewpoint of the energy spectrum, shown in Fig. 6, both have a somewhat similar slope, except that their theory predicts a smaller energy of turbulence at t = 1. The same tendency is also seen in the numerical experiment performed by Jeng et al,[18] although their result is not plotted in the figure in order to avoid complication. It may be noted, however, that their experiment is very similar to the present calculation, in that both deal with the operator T^t in (1.2) exactly and both try to compute an average property for an ensemble of initial velocity fields by sampling. But Jeng et al. limited the ensemble to one special type, made up from n independent

uniform random numbers (n seems to be 50, judging from an illustration in their paper), so that $\phi(y_0, 0)$ in their case has a form quite different from that of (1.7). Furthermore, in order to calculate the statistical properties of the velocity field, they appealed to the operation of space averaging (assuming statistical homogenity and the so-called ergodic hypothesis) rather than averaging over a large number of members of the ensemble. These facts give their experiment a flavor quite different from our approach. If they had simply proceeded with the latter averaging operation, they would not have needed any hypothesis beforehand but, after making sure of the reliability of their samplings, should have been able to prove it. In spite of these rather great differences between their method and ours, it is notable that the k^{-2} spectrum law is qualitatively recovered by both. It would be even more interesting if it were known what result they had for the feature of energy decay, because a comparison with Fig. 1 would then show how the result is affected by the initial condition on ϕ.

It is worth noting that all energy spectrums in Fig. 6 tend to almost the same value as $k \to 0$, regardless of t and R. This value may be estimated from the theoretical curve at $t = 0$, giving

$$E(0, 0) = \frac{1}{\pi} \int_0^\infty e^{-r^2} \, dr = \pi^{1/2}/2. \tag{3.2}$$

This fact is consistent with the existence of the so-called Loitsianski constant for Burgers' model of turbulence.[2,13] We have verified that at $k = 0$ our results

for different t and R recover the value (3.2) with a relative error of less than 5%. This may be considered as another measure of the order of accuracy of our Monte Carlo quadrature.

iii) Deviation from normality

It is hard to make a decisive quantitative statement on the extent to which our probability distribution functional of the velocity field deviates from normality, because we must always take into account the error intrinsic to Monte Carlo quadrature. To determine this deviation, we must deal with a correlation whose order is higher than two, and the higher the order of correlation dealt with, the larger would the value of N be needed in order to keep enough accuracy. Fig. 7 shows the result of calculating, at N = 30, the curtosis for many values of R and t. In our case, the curtosis at t = 0 should be exactly 3, since we have started from a normal distribution. The only plausible conclusion, therefore, is that there is a tendency for the curtosis to decrease very slightly with increasing time, i.e. for the distribution to become slightly flatter, at least for R greater than or equal to 1. Calculated values of the skewness factor are distributed almost randomly about zero; hence it may be concluded that there is no significant deviation from the zero value.

iv) Time-development of an individual velocity field

Finally it is worthwhile to look into the behavior of a typical individual velocity field. Fig. 8 shows the time development, for R = 100 and N = 30, of the

particular velocity field which at the initial time was made up from a certain set of standard normal random numbers, plotted over the interval [-2.5, 2.5]. (Actually, the random numbers in this case are taken between the 61st and the 120th of those generated by Kronmal's method.[12] The general feature of an individual velocity field was unchanged even if another set of random numbers was taken.) At t = 1 a shock-like sharp discontinuity can already be observed; it moves along according to its own dynamics,[2] but diminishes gradually because of the relatively predominating (with decay) viscous effect. What Burgers[2] calls the hinge point around which the curve of u(x) rotates in a clockwise fashion with time, can be seen at $x \doteq 2.3$. Another hinge point at $x \doteq -3.6$ is predicted. The slope of u(x) appears to be almost $(t + t_0)^{-1}$ near the hinge point and, for $t \gtrsim 1$, to be so everywhere except near a rounded shock-like region. (In this example $t_0 \doteq 1$.)

For high Reynolds number, these features identify the reality of Burgers' conception of the development of an individual velocity field pretty well. The period with $t \gtrsim 1$ seems to be suitable for application of his simplified statistical assumption except for the rounded shock-like regions. For comparison, the calculated time development for R = 1 of the same initial velocity field is shown in Fig. 9. In this case the diffusive action due to viscosity predominates for all periods of time. The contrast with the former case is very remarkable.

4. Conclusion

This work verified that the functional integral expression for the correlation function of the turbulent velocity field, derived from the Hopf formalism for turbulence,[3] is directly calculable through the introduction of the functional integration technique given by (1.3)-(1.6) and the use of Monte Carlo quadrature.

The present numerical result for the Burgers' model turbulence in the infinite domain of x is accurate enough to reveal a reasonable transition in the features of energy decay as R changes. For R less than 1 the turbulence energy decays just as the linear theory predicts over a considerable period of time, while for R greater than 1, the decay pattern changes rapidly with R so that even for $R = 10$ it is almost in accord with the predicted asymptotic ($R \to \infty$) pattern (at least until $t = 100$). Although the time-dependence of the asymptotic decay pattern is not in accord with the results of other approximate theories, except for Burgers', the energy spectrum at some instants in some wave-number regions has a tendency to behave at least qualitatively according to the k^{-2} spectrum law, which is well predicted by all these theories including Burgers'.

When the operator T^t is not known explicitly, as is the case with the Navier-Stokes turbulence, we seem to face some difficulty in extending this functional approach. But it can still be used if $T^t\ u$ is developed as

$$u(x,\ t) = \sum_k b_k(t)\ s_k(x)$$

(Cf. (2.1)), where both x and u are vectors, provided that the time-development of $\{ b_k(t) \}$ can be computed. This means that the T^t is given numerically. Thus it may be expected that the present method of computation on the exact ensemble-mechanical basis will further contribute to the checking of the validity of approximate theories and will give typical data for engineering purposes.

Appendix

The average velocity field U(x) and the covariance function Q(x, x') are defined by the following equations:

$$U(x) = \int_{\Omega} u(x)\, p(u)\, \delta u, \tag{A1}$$

$$Q(x,\ x') = \int_{\Omega} \{U(x) - u(x)\}\ \{U(x') - u(x')\}\ p(u)\ \delta u, \tag{A2}$$

where p(u) is the probability density for u in the symbolic sense. We also have

$$1 = \int_{\Omega} p(u)\ \delta u\,. \tag{A3}$$

Under the conditions (A1)-(A3), let us try to make the information entropy a maximum, where the information entropy is defined by the limit of

$$S^{2N} = -\int_{\Omega} p(u^{2N})\ \log p(u^{2N})\ \delta u^{2N}/2N \quad \text{as} \quad 2N \to \infty, \tag{A4}$$

according to Shannon.[19] The Lagrange multiplier method for the variational problem leads to the equation

$$0 = -\int_{\Omega} \delta u \left[\{\log p(u) + 1\} + \int a(x)\, U(x)\, dx + \iint b(x, x')\, \{U(x) - u(x)\}\, \{U(x') - u(x')\}\, dx\, dx' - c \right]. \tag{A5}$$

Here a(x), b(x, x') and c are the undetermined multipliers. As a result,

$$p(u) = e^{c-1} \cdot \exp\left[- \int a(x)\, U(x)\, dx - \iint b(x, x')\, \{U(x) - u(x)\}\, \{U(x') - u(x')\}\, dx\, dx' \right], \tag{A6}$$

where b(x, x') is assumed to be positive definite. The Fourier transformation of this is, in general,

$$\phi(y) = C \exp\left[\int A(x)\, y(x)\, dx - \iint B(x, x')\, y(x)\, y(x')\, dx\, dx' \right], \tag{A7}$$

where A(x), B(x, x') and C are related to a(x), b(x, x') and c, and should be determined in such a way that ϕ and p are consistent with the conditions (A1)-(A3). Remembering the properties of the characteristic functional ϕ, we can obtain

$$\left.\begin{aligned} A(x) &= i\, U(x) \\ B(x, x') &= (1/2)\, Q(x, x') \\ C &= 1. \end{aligned}\right\} \tag{A8}$$

Acknowledgment

The senior author is grateful to Prof. J. M. Burgers of The University of Maryland for an enlightening discussion. The authors are also indebted to Dr. J. C. Hill for his comments and to Mr. R. C. Lee for his editorial assistance. The work was supported by the National Academy of Sciences.

References

1. I. Hosokawa, Phys. Fluids 11, 2052 (1968).

2. J. M. Burgers, Proc. Acad. Sci. Amsterdam 53, 247, 393, 718, and 732 (1950); for further statistical development see J. M. Burgers in Nonlinear Problems of Engineering, edit. by W. F. Ames (Academic Press, New York, 1964), p. 123.

3. E. Hopf, J. Rat. Mech. Anal. 1, 87 (1952).

4. V. Volterra, Theory of Functionals and of Integral and Integrodifferential Equations (Dover Pub., New York, 1959).

5. I. Hosokawa, J. Math. Phys. 8, 221 (1967).

6. P. R. Halmos, Measure Theory (D. Van Nostrand Co., Princeton, 1950).

7. E. Hopf, Commun. Pure Appl. Math 3, 201 (1950).

8. J. D. Cole, Quart. Appl. Math. 9, 225 (1951).

9. The idea of adopting the most unbiased initial condition in statistical-physical theory is discussed by S. Gartenhaus, Elements of Plasma Physics (Holt, Rinehart and Winston, Inc., New York, 1964), Chap. 3.

10. K. D. Friedrichs et al., lecture notes, Courant Institute of Mathematical Sciences, New York Univ. (1959).

11. J. M. Hammersley and D. C. Handscomb, Monte Carlo Methods (John Wiley and Sons, New York, 1964).

12. R. Kronmal, J. Assoc. Comput. Machinery 11, 357 (1964).

13. W. C. Meecham and A. Siegel, Phys. Fluids 7, 1178 (1964).

14. S. A. Orszag and L. R. Bissonnette, Phys. Fluids 10, 2603 (1967).

15. R. H. Kraichnan, Phys. Fluids 11, 265 (1968); T. Tatsumi, Phys. Fluids, to be published.

16. Z. Kopal, Numerical Analysis (John Wiley & Sons Inc., New York, 1961), p. 408.

17. P. G. Saffman, in Proceedings of the International School of Nonlinear Mathematics and Physics, edit. by M. D. Kruskal et al (Springer Verlag, Berlin, 1967).

18. P. T. Jeng, R. Forester, S. Haaland and W. C. Meecham, Phys. Fluids 9, 2114 (1966).

19. C. E. Shannon and W. Weaver, The Mathematical Theory of Communication (Univ. of Illinois Press, Urbana, 1964).

Figure Captions

Fig. 1. Features of the energy decay

Fig. 2. Average values for $\langle [u(0)]^2 \rangle_t$ versus the number of samples at various instants, with R = 100, N = 30.

Fig. 3. Dependence of the energy decay on N, with R = 100.

Fig. 4. Correlation function $\langle u(0)\, u(x) \rangle_t$ for various values of R and t, with N = 30.

Fig. 5. Average values for $\langle u(0)\, u(x) \rangle$ at t = 1 versus the number of samples at various distances, with R = 100, N = 30.

Fig. 6. Energy spectrums E(k, t) for various values of R and t, with N = 30.

Fig. 7. Curtosis as a function of time for various R.

Fig. 8. Time development of a particular velocity field for R = 100.

Fig. 9. Time development of a particular velocity field for R = 1.

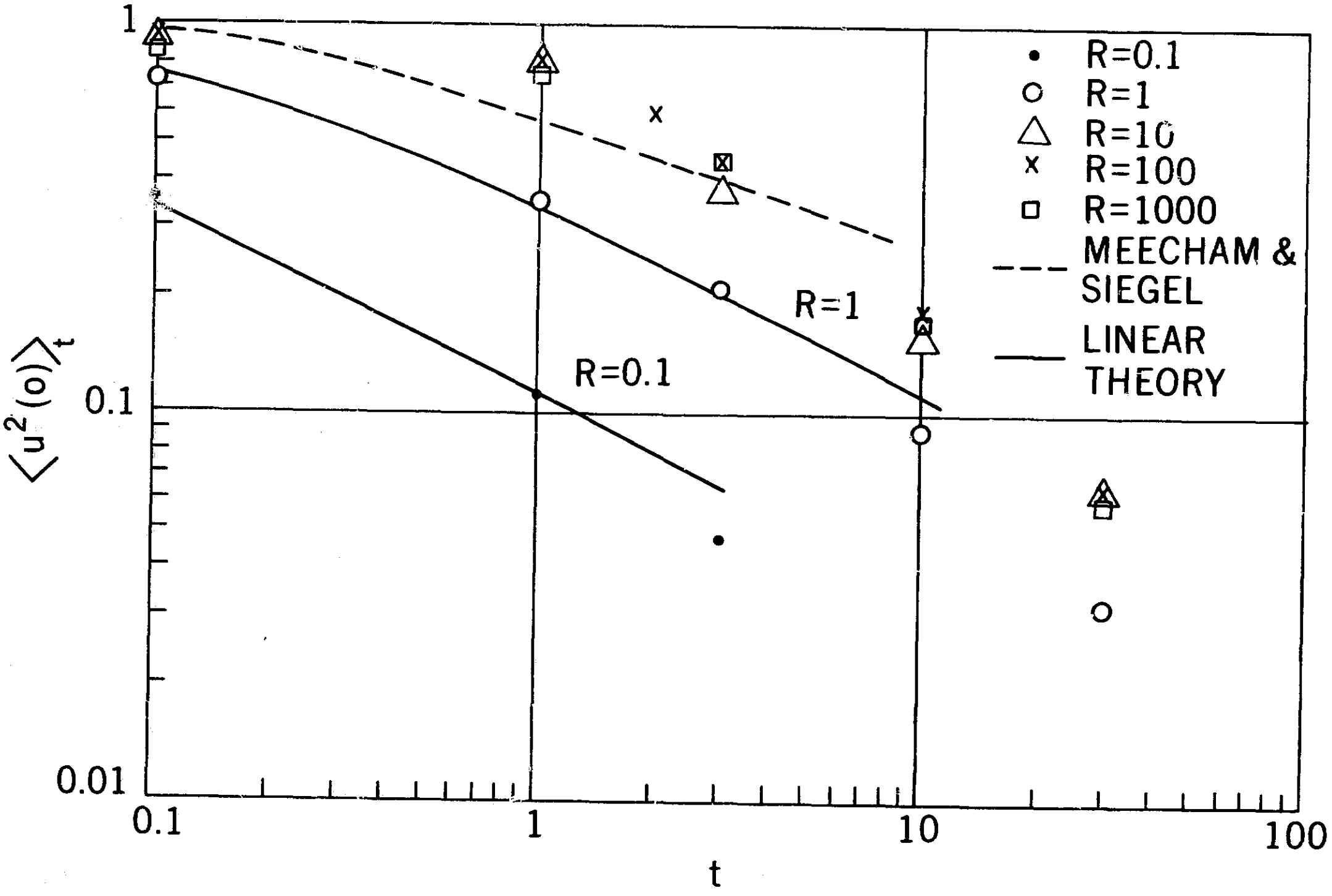
1
0.1
0.01
0.1
1
10
100
t
$\langle u^2(o) \rangle_t$
R=0.1
R=1
R=10
R=100
R=1000
MEECHAM & SIEGEL
LINEAR THEORY
R=1
R=0.1

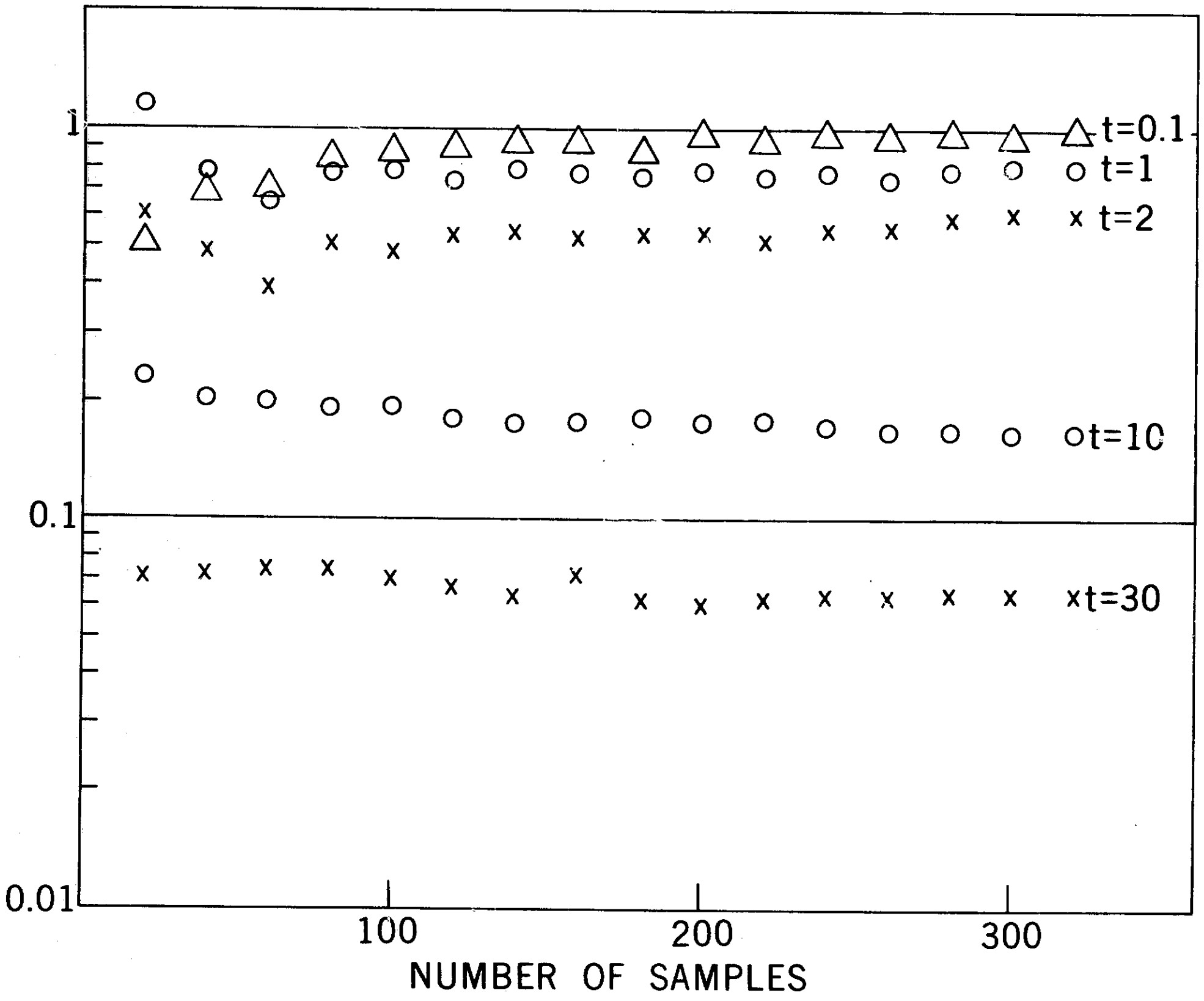
1
0.1
0.01
$\langle u^2(o) \rangle_t$
t=0.1
t=1
t=2
t=10
t=30
100
200
300
NUMBER OF SAMPLES

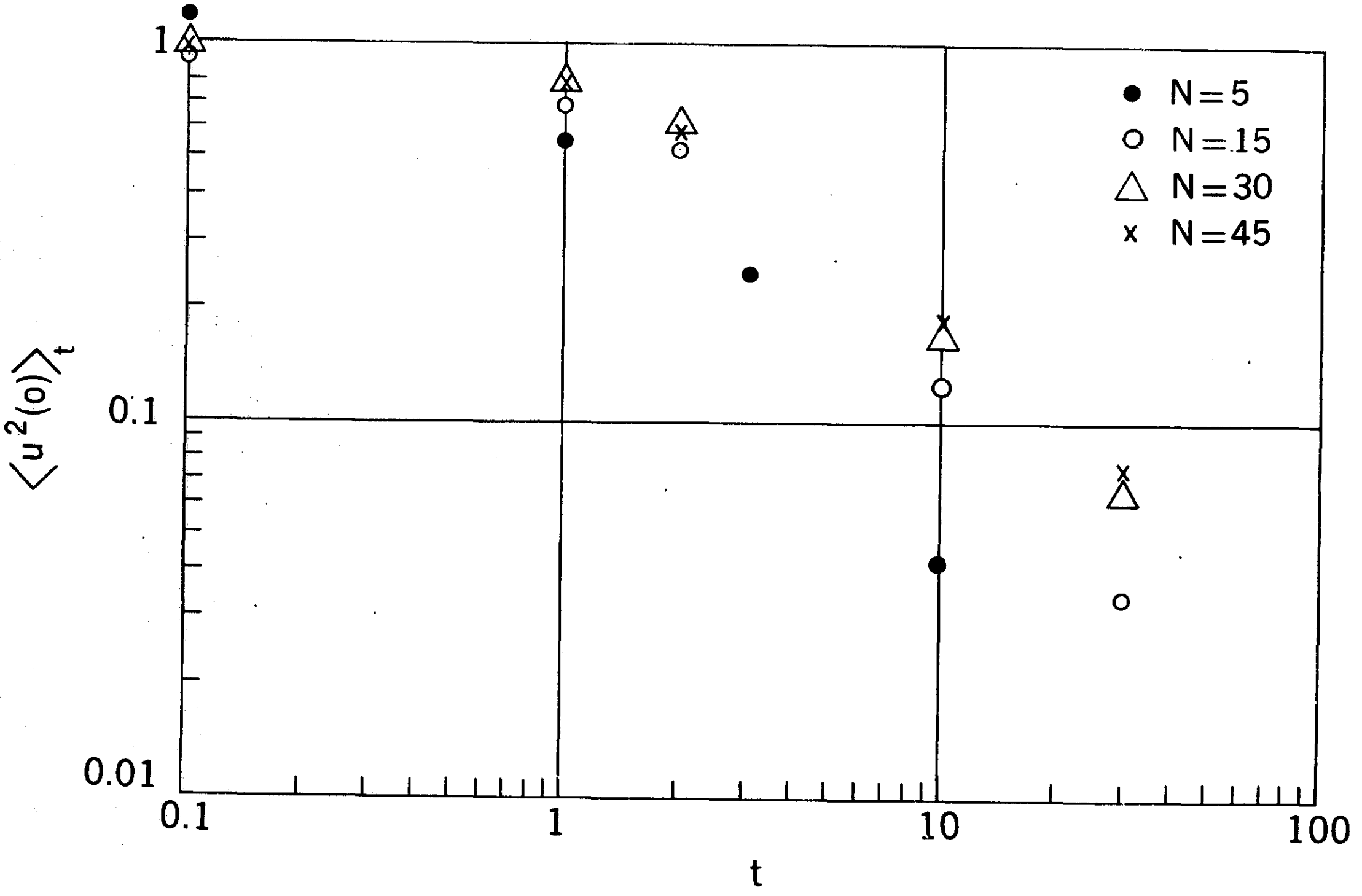
1
0.1
0.01
0.1
1
10
100
t
$\langle u^2(o) \rangle_t$
N=5
N=15
N=30
N=45

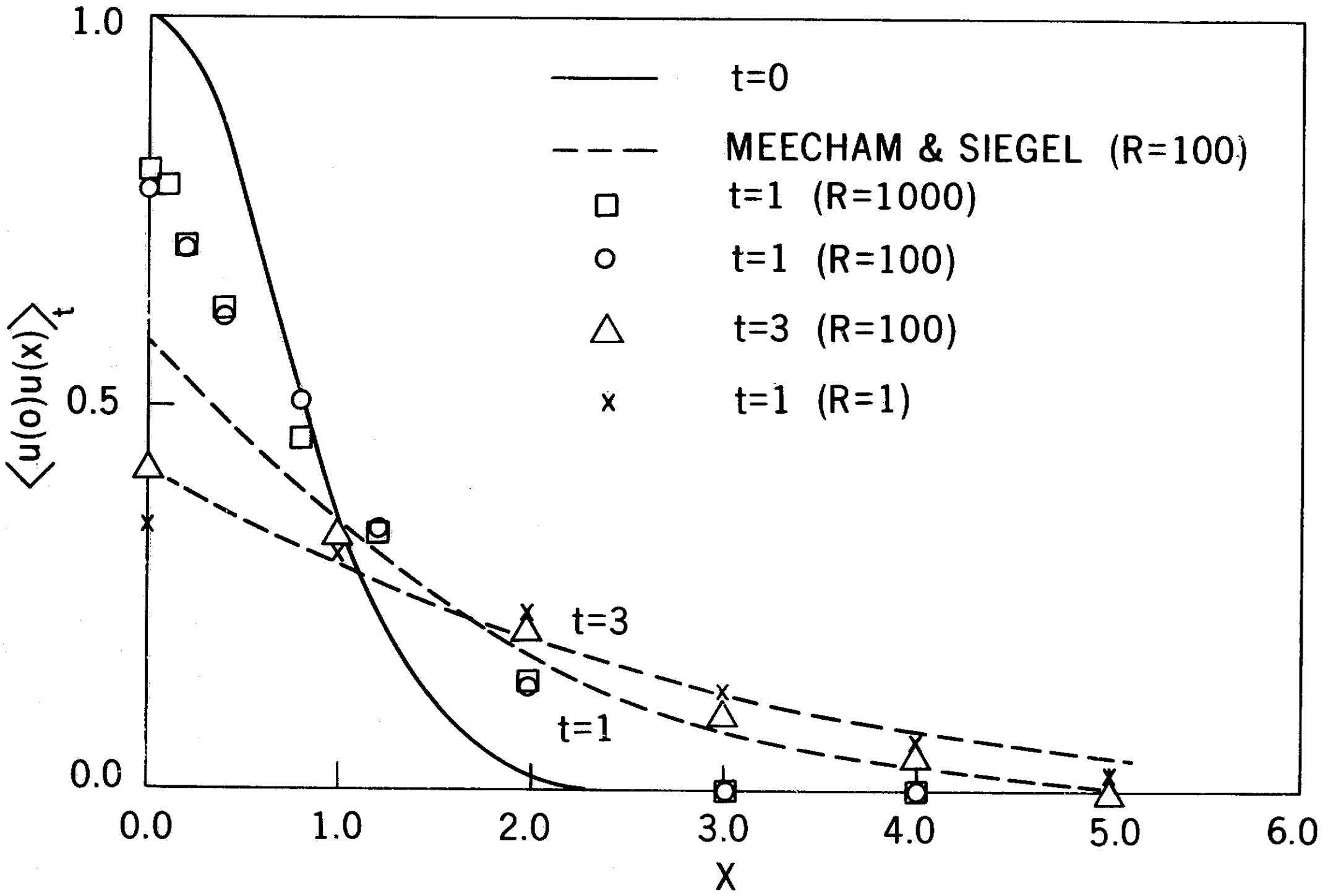
1.0
0.5
0.0
$\langle u(o)u(x)\rangle_t$
t=0
MEECHAM & SIEGEL (R=100)
t=1 (R=1000)
t=1 (R=100)
t=3 (R=100)
t=1 (R=1)
t=3
t=1
0.0
1.0
2.0
3.0
4.0
5.0
6.0
X

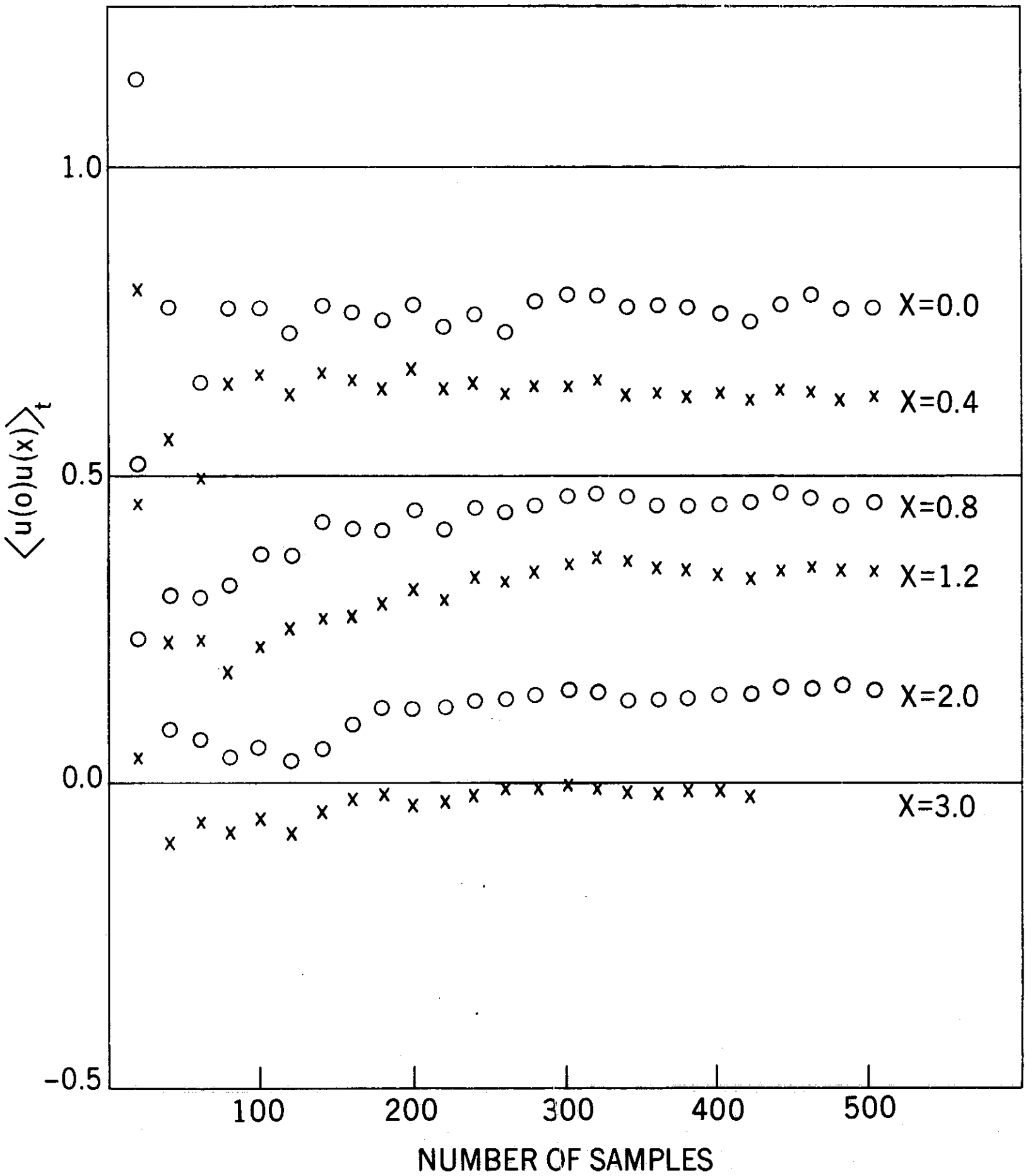
1.0
0.5
0.0
-0.5
100
200
300
400
500
NUMBER OF SAMPLES
$\langle u(o)u(x)\rangle_t$
X=0.0
X=0.4
X=0.8
X=1.2
X=2.0
X=3.0

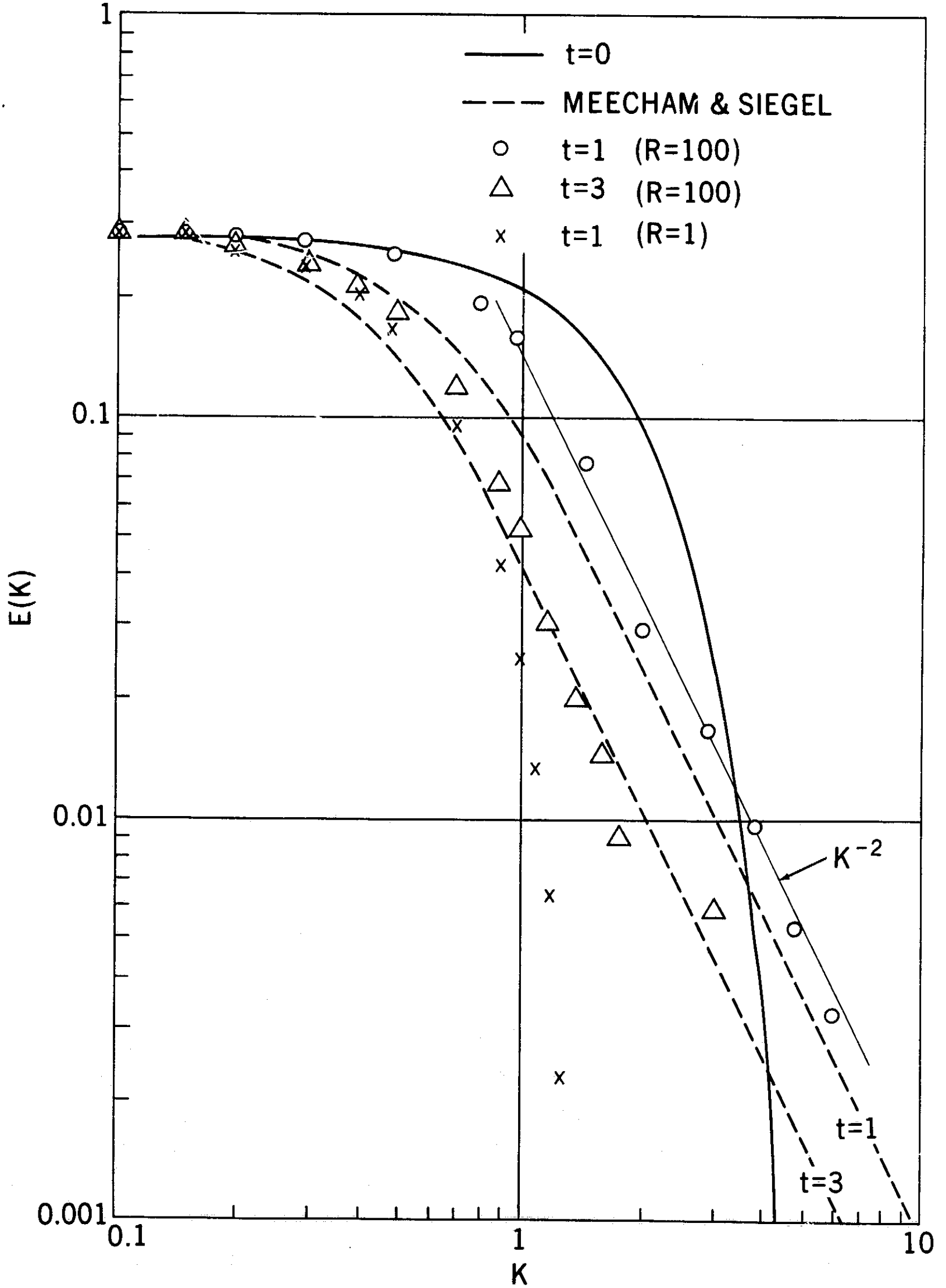
t=0
MEECHAM & SIEGEL
t=1 (R=100)
t=3 (R=100)
t=1 (R=1)
E(K)
K
1
0.1
0.01
0.001
0.1
1
10
K^{-2}
t=1
t=3

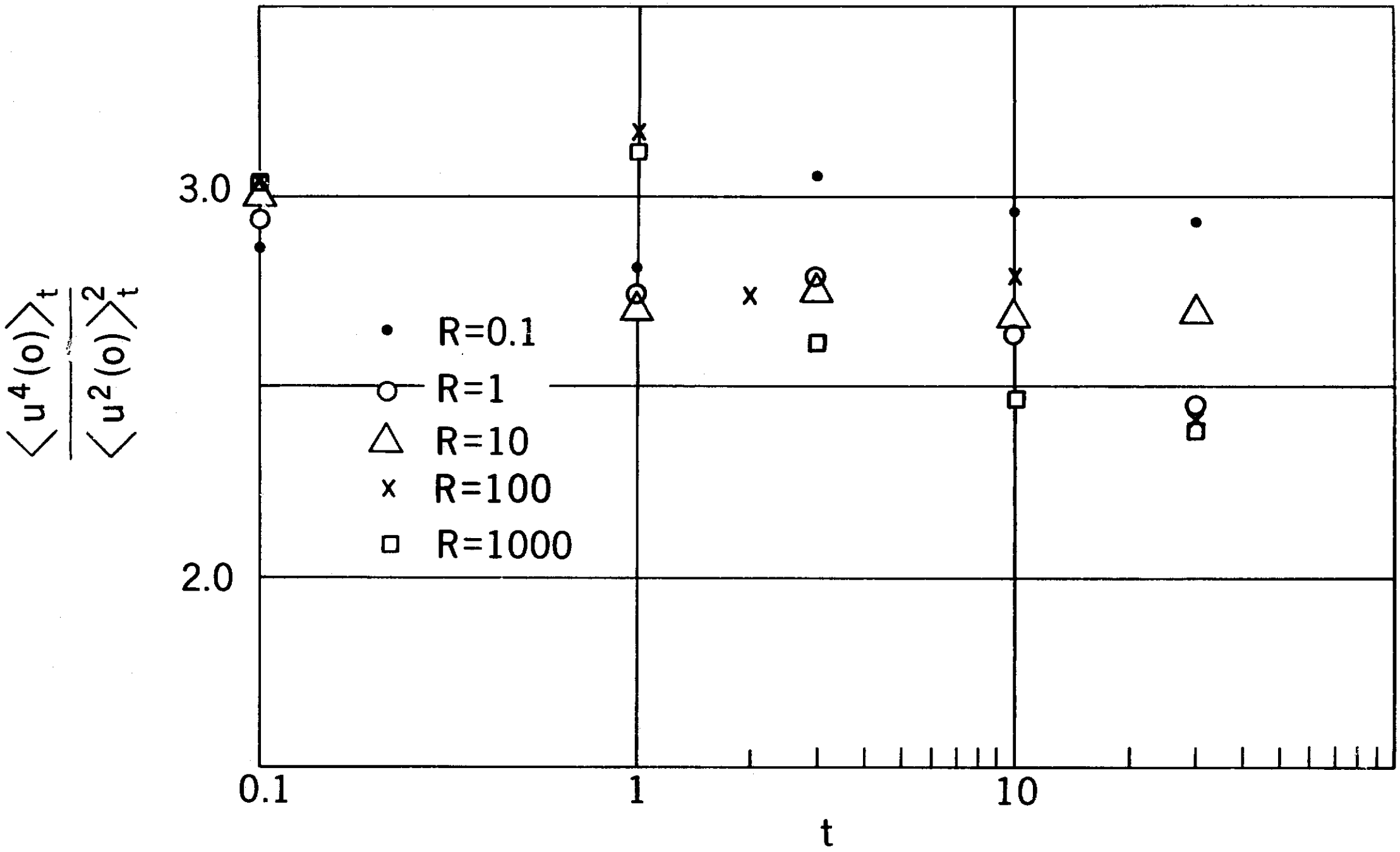
$\frac{\langle u^4(o)\rangle_t}{\langle u^2(o)\rangle_t^2}$
3.0
2.0
R=0.1
R=1
R=10
R=100
R=1000
0.1
1
10
t

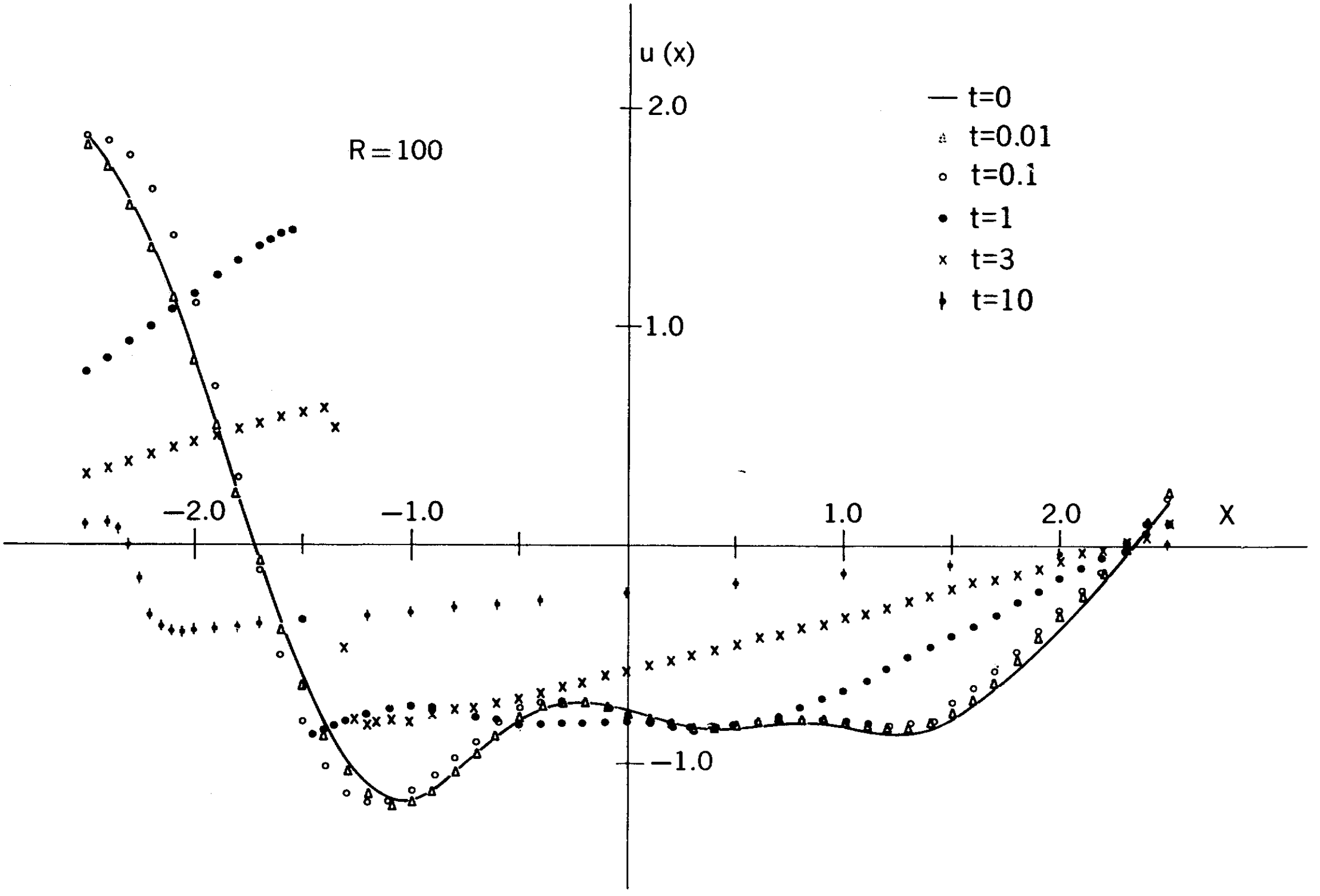
u (x)
2.0
1.0
−1.0
R = 100
−2.0
−1.0
1.0
2.0
X
t=0
t=0.01
t=0.1
t=1
t=3
t=10

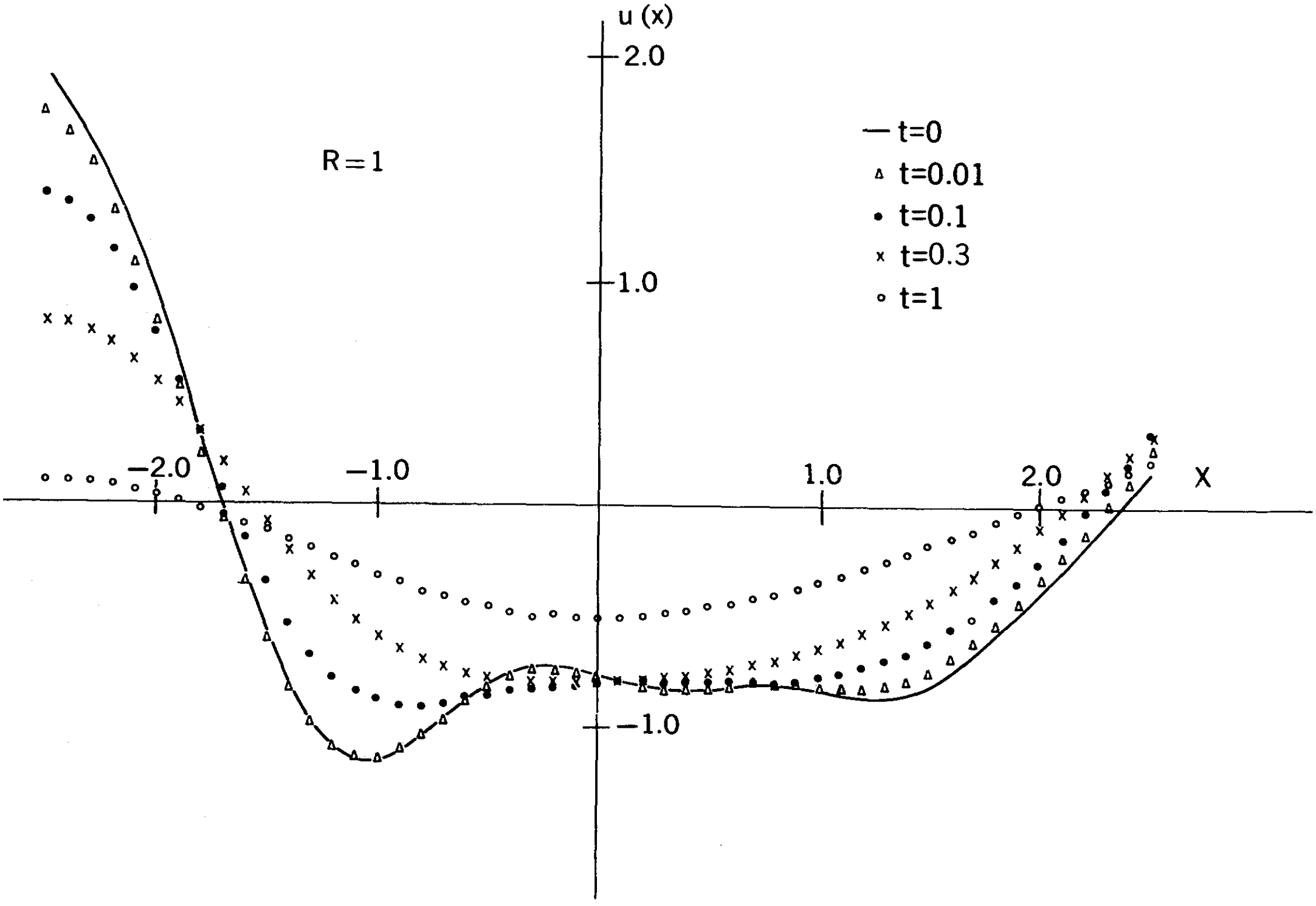
u (x)
2.0
1.0
−1.0
−2.0
1.0
2.0
X
−1.0
R=1
— t=0
Δ t=0.01
• t=0.1
x t=0.3
∘ t=1